JOURNAL OF GEOPHYSICAL RESEARCH, VOL. 103, NO. D14, PAGES 17,129–17,147, JULY 27, 1998

Physicochemistry of aircraft-generated liquid aerosols, soot, and ice particles
2. Comparison with observations and sensitivity studies

B. Kärcher, R. Busen, A. Petzold, F.P. Schröder, and U. Schumann

Deutsches Zentrum für Luft- und Raumfahrt, Institut für Physik der Atmosphäre, Wessling, Germany

E.J. Jensen

NASA Ames Research Center, Moffett Field, California

Abstract. Results from a coupled microphysical-chemical-dynamical trajectory box model have been compared to recent in situ observations of particles generated in the wake of aircraft. Sulfur emissions mainly cause the formation of ultrafine volatile particles in young aircraft plumes (mean number radius $\sim 5\,\mathrm{nm}$). Volatile particle numbers range between 10^{16} and 10^{17} per kg fuel burnt for average to high fuel sulfur levels, exceeding typical soot emission indices by a factor of 10–100. Model results come into closer agreement with observations when chemi-ions from fuel combustion are included in the aerosol dynamics. Ice particles (mean number radius $< 1\,\mu\mathrm{m}$) in young contrails mainly nucleate on water-activated exhaust aerosols. Homogeneous freezing and soot-induced heterogeneous freezing are competitive processes leading to ice formation, depending on the temperature and level of oxidized sulfur species. There is evidence that soot triggers freezing even for low fuel sulfur contents, suggesting a sulfur-independent water activation pathway. Metal particles emitted by jet engines and entrained ambient aerosols may contribute to the formation of larger ($> 1\,\mu\mathrm{m}$) crystals. Contrails with larger crystals would also form without soot and sulfur emissions. The lifecycle of cirrus clouds can be modified by exhaust aerosols.

1. Introduction

In the companion paper [*Kärcher*, this issue (hereinafter referred to as part 1)] we have emphasized the obvious lack of knowledge about particle formation in jet aircraft plumes and how dynamical and physicochemical processes alter the new and emitted aerosol particles. The objective of the present paper is to explore this issue by analyzing data from in situ observations in young plumes (plume age below a minute).

We base our comparisons mainly on measurements made during the five SULFUR missions [*Busen et al.*, 1997] which aimed at investigating contrail formation and its dependence on the fuel sulfur content (FSC). Also, data from other missions (SUCCESS, Toon et al. in the work of *Thompson et al.* [1996]; POLINAT, *Schumann et al.* [1997]) are compared with model results. In addition, we will present sensitivity studies that yield implications for the evolution of liquid and solid particles which cannot be assessed by present observations.

Paper number 98JD01045.
0148-0227/98/98JD-01045$09.00.

It turns out to be difficult to isolate and quantify details of plume microphysics by such comparisons. One reason for this difficulty lies in measurement limitations. Just to name one, we mention the uncertainty in detection limits of condensation nuclei counters for nanometer-sized particles that become of importance under plume conditions. Also, unknown engine emission properties to be prescribed as initial conditions in the simulations do not allow to draw unambigous conclusions. Here we mention possible emissions of SO_3, an important aerosol precursor. A detailed understanding of plume aerosol processes is further complicated by the variability of thermodynamic properties in the turbulent wake. These inhomogeneities directly translate into pronounced variabilities of measured parameters on timescales $\sim 1\,\mathrm{s}$ and spatial scales $\sim 1\,\mathrm{m}$. Finally, we point out existing uncertainties in the underlying model microphysics (e.g., nucleation rates).

In spite of these caveats we attempt to critically asssess the capability of our simulation model to predict the formation and evolution of aircraft-generated aerosols and contrails. Some conclusions can be drawn with fairly high confidence, but also outstanding open issues arise from the comparisons, both of which are summarized at the end of the paper.

2. Observations During SULFUR 1 and 2

We compare results from our plume aerosol simulation model with in situ observations of contrails performed during the SULFUR 1 [*Busen and Schumann*, 1995] and SULFUR 2 [*Schumann et al.*, 1996] missions. In both missions, the two jet engines of the Deutsches Zentrum für Luft- und Raumfahrt (DLR) research aircraft ATTAS were fueled with kerosene containing different sulfur levels. In the SULFUR 1 experiment, very low and average FSCs (0.002 g S and 0.26 g S per kg fuel) was used. In the SULFUR 2 experiment, the kerosene contained either low and very high sulfur contents (0.17 g S and 5.5 g S per kg fuel). The very low level is still much higher than typical SO_2 volume mixing ratios in the upper troposphere (around 100 ppt, but with considerable variability between 10 and 400 ppt; see *Langner and Rhode* [1991]). The very high sulfur level is nearly twice as large as the internationally accepted maximum value for the sulfur mass in kerosene.

The use of different FSCs in engines of the same aircraft under identical ambient conditions and engine parameters allows us to focus on the pure sulfur effects on contrail formation. It has been pointed out earlier that a visible contrail does not form under the assumption that the contrail particles stay liquid [*Kärcher et al.*, 1995; *Schumann*, 1996a]. Rather, contrails become visible when particles pass a liquid growth stage and freeze subsequently as water ice [*Kärcher et al.*, 1996], which is plausible given the low temperatures at the flight levels which are typically below the spontaneous freezing temperature of water droplets ($\sim 40°$ C). The latter authors also found that soot must be involved in ice formation under threshold conditions. For given pressure and relative humidity at the flight level the overall propulsion efficiency of the cruising aircraft, and fuel properties, the threshold temperature T_{th} at which a contrail just becomes visible can be calculated following *Schumann* [1996b]. Exactly at threshold, liquid water saturation is reached in the diluting plume due to mixing of the hot and humid exhaust with ambient air.

The SULFUR 1 experiment was made at ambient pressure $p_a = 302$ hPa, temperature $T_a = 223.45 \pm 0.5$ K, and relative humidity RH $\simeq 34\,\%$ that just allowed the formation of optically visible ice particles. In this threshold case, corresponding to $T_{th} = 223.2$ K, the humidity was estimated from nearby radiosoundings and could have been $\sim 10\,\%$ higher, in which case $T_{th} = 223.7$ K. No visible difference was found between the onset and the color of both very short-lived contrails. A recent analysis of observed contrails by *Jensen et al.* [1998] confirmed that liquid water saturation must be reached in the plume in order to produce a visible contrail. Our simulations yield a maximum plume relative humidity of 103 % (including water condensation) using $T_a = 222.95$ K and RH = 45 %, but the simulated plume stayed water subsaturated (peak humidity 95 %) for $T_a = 223.45$ K and RH = 34 %. We therefore use the former set of input data in the calculation.

The SULFUR 2 experiment was made several degrees below the threshold formation temperature at $p_a = 287$ hPa, $T_a = 218$ K, and RH = 40 %, corresponding to $T_{th} = 223.5$ K. In this case, a visible difference was observed between the contrails. The ice particles formed behind the engine with very high-sulfur loading were earlier visible by 5 – 8 m than the contrail originating from low-sulfur fuel. The contrails were also short-lived but were observed longer (plume age 20–30 s) than in the SULFUR 1 case. The difference in color between both contrails which was observed has been explained by *Gierens and Schumann* [1996] by freezing of more and correspondingly smaller ice particles in the high-sulfur contrail compared to the low-sulfur contrail. This is consistent with the fact that the ice particles in the high-sulfur contrail evaporated faster than those in the other contrail.

Petzold and Schröder [1998] and *Petzold et al.* (manuscript in review, 1998) characterized the ATTAS soot particles in ground tests (SULFUR 3) and in-flight (SULFUR 5) experiments using a passive cavity (PCASP) and a forward scattering aerosol spectrometer probe (FSSP), a condensation nuclei (CN) counter, and filter sampling techniques. Together, the soot measurements behind the ATTAS engine both at ground and in flight constitute a self-consistent data set. The soot size distribution can be approximately represented by adding two lognormal modes. The primary (secondary) mode is characterized by a nozzle exit plane number density of 4×10^6 (1.5×10^4) cm^{-3}, a mode radius of 25 (100) nm, and a geometrical width of 1.56 (1.65). These numbers are consistent with the measured soot masses and the total nonvolatile CN number densities (scaled to exit conditions) within experimental uncertainties and correspond to 1.7×10^{15} soot particles per kilogram fuel, or 0.2 g / kg using the engine flow parameters recorded during the SULFUR 1 observations. During SULFUR 2, *Schumann et al.* [1996] inferred comparable numbers from the in-flight measurements behind the ATTAS.

2.1. Numerical Simulations

In addition to the size and abundance of the ATTAS soot aerosols, we have to prescribe abundances of oxidized sulfur gases and chemi-ions to initialize the model.

Brown et al. [1997] predicted fuel sulfur-dependent emission of SO_3 molecules for the ATTAS jet engines, reaching exit plane values of $s = [SO_3]/([SO_2]+[SO_3])$ up to 0.04, by simulating gas phase chemistry in the turbine flow. We use a constant value $s = 0.02$ for the ATTAS as input to our model. *Yu and Turco* [1997] and *Arnold et al.* [1998] pointed out the possible importance of chemi-ions from jet fuel combustion in the nucleation and growth of the volatile plume aerosols. Emissions and evolution of chemi-ions are treated approximately in this work, as described in part 1. At threshold, only

moderate water supersaturations ($\leq 3\,\%$) are reached in the plume. The small ($< 5\,$nm) chemi-ion mode can probably not be activated to grow into water droplets and freeze in the presence of coated soot particles that freeze slightly earlier in the very low (0.002 g S per kg fuel) case due to the missing condensational growth of the ions by condensation of H_2SO_4. Therefore we neglect chemi-ions for simulations with very low FSC but take them into account in all other cases. The role of ions and volatile aerosols in contrail formation is discussed in more detail in section 3.2.

To compute the heterogeneous nucleation rates of ice in the solution droplets in the presence of a soot surface, we prescribe a contact angle $\vartheta = 110°$ between the ice germ and the soot surface. As we will show below, this leads to a consistent interpretation of the contrail observations for low to very high fuel sulfur levels. *Kärcher et al.* [1996] have measured the contact angle $53° - 66°$ of a 50-wt % H_2SO_4/H_2O droplet on a graphitic surface (mimicking dry, unactivated soot), depending on the degree of OH radical exposure of the surface prior to the contact angle measurement. The lower values were measured on the OH-treated soot surface. Interestingly, similar observations have been made by *Kotzick et al.* [1997], who report an upper limit of 50° for carbon particles wetted with liquid water; the contact angle decreased to 26° on ozone-treated carbon aerosols. A higher contact angle for an ice germ on soot may be expected due to the apparently higher crystallographic misfit between a soot surface and an ice germ nucleating on it compared to a liquid germ or droplet. The value of ϑ is the most sensitive parameter in the calculation of the nucleation rate. Decreasing ϑ enhances heterogeneous freezing rates and lessens the role of homogeneous freezing in contrail formation, when both processes become competitive in contrail formation.

The radial size distributions $dn/d\log(r)$ of volatile aerosols (subscript d), soot (s), and ice particles (i) simulated by the plume aerosol model described in part 1 are shown in Figure 1 at a plume age of 1 s. Table 1 contains relevant microphysical data of contrail particles taken from the simulations. At this plume age, the new contrails have formed and condensed the emitted water vapor [*Kärcher et al.*, 1996]. Background aerosols definitely had no effect in the SULFUR 1 case due to the low abundance ($10\,\mathrm{cm}^{-3}$) and also played a minor, if any, role in the SULFUR 2 case. They are therefore omitted in these calculations.

The abundance of volatile aerosols $> 1 - 2\,$nm shown in Figure 1a clearly increases with increasing FSC. Note that the size spectrum in the very low sulfur case (obtained without chemi-ions, as noted above) is not visible, for it is located at $r < 1\,$nm. This dependence can be inferred from Figure 1a by comparing the solid curve with the long-dashed curve, and the dotted-dashed curve with the short-dashed curve. By comparing the 0.17 g/kg case at $T_a = 218\,$K with the 0.26 g/kg case at 223 K, it is also seen that the

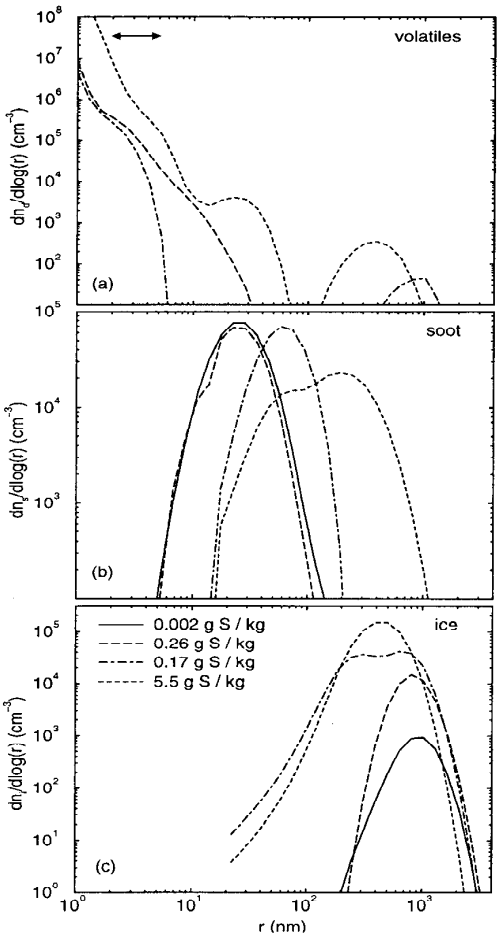

Figure 1. Modeled size distributions of (a) volatile aerosols, (b) soot, and (c) contrail ice particles in the observed plume of the DLR ATTAS after freezing at a plume age of 1 s, or 230 m past exit. The sulfur levels (see legend) were 0.002 g S per kg fuel (very low) and 0.26 g/kg (average) in the SULFUR 1 experiment ($T_a = 223\,$K), and as 0.17 g/kg (low) and 5.5 g/kg (very high) in the SULFUR 2 experiment (218 K). All calculations except the very low sulfur case include the effects of chemi-ions on volatile aerosol growth and freezing processes. Background aerosols are neglected in the calculations due to their negligible abundance (compared to plume aerosols) during the measurements. The arrow in Figure 1a marks typical lower detection limits of particle counters.

volatile aerosol abundance tends to increase with decreasing ambient temperature due to increased nucleation and growth rates. The spectra in Figure 1a are somewhat broadened due to numerical diffusion effects (see part 1), which however does not affect these principle trends. Only the largest ($> 4\,$nm) plume aerosols can be activated (i.e., grow by rapid water uptake) and participate in ice formation, especially at low temperatures and/or high sulfur levels; see ζ(hom) and ζ(het)

Table 1. Numerical Simulation Results of Contrail Properties in the Exhaust Plume of the DLR ATTAS at a Plume Age of 1 s for Different Sulfur-Containing Fuels.

Fuel S, g/kg	ζ(hom)	ζ(het)	$\bar{r}_i$, μm	τ	$n_d^>$, cm^{-3}	n_s, cm^{-3}	n_i, cm^{-3}
0.002[a]	0	1	0.96	5(−4)[c]	1.0(−7)	8.5(+4)	1.0(+3)
0.26[a]	0.002	0.998	0.87	6(−2)	2.1(+4)	7.1(+4)	1.1(+4)
0.17[b]	0.440	0.560	0.54	0.7	3.0(+3)	7.0(+4)	6.5(+4)
5.5[b]	0.570	0.430	0.45	1.3	1.4(+5)	4.4(+4)	1.5(+5)

Shown are the abundances ζ(hom) (ζ(het)) of homogeneously (heterogeneously) frozen contrail ice particles in fractions of total ice number density; the average radius (first moment of the size spectrum) of the ice particles $\bar{r}_i$; and the optical depth τ of the contrails at 0.55 μm wavelength one wingspan ($\simeq$ 30 m) behind the airplane; number density $n_>$ of volatile aerosols (d) with radii > 4 nm (detectable by a CN counter), and total number densities of soot (s) and ice particles (i). The 0.002 g S per kg fuel case was simulated without ion effects. Contrails become visible for $\tau > 0.03$. Read 1.0 (−7) as 1.0×10^{-7}.

[a] Values (very low and average) from observations during SULFUR 1, where contrails formed under threshold conditions at 223 K.

[b] Values (low and very high) from observations during SULFUR 2, where contrails formed below the threshold conditions at 218 K.

[c] Simulated contrail is invisible.

in Table 1. (Numerical diffusion may cause enhanced growth of volatiles across the critical water activation size; therefore ζ(hom) values are upper limits.) Interestingly, for 0.17 g/kg and 5.5 g/kg some of these activated droplets stay unfrozen around 0.3 − 1 μm radius, indicating a rapid termination of the freezing processes.

Figure 1b shows the soot size distributions for the different cases. Increasing the abundance of reactive sulfur gases, and thereby also of volatile aerosols, leads to an enhanced growth of the liquid coating on the soot particles (compare part 1). This effect is most pronounced between low and very high fuel sulfur levels, compare the dotted-dashed with the short-dashed curve. In the SULFUR 1 cases, soot is found to be the only particle type being able to produce a significant number of ice particles (see long-dashed line in Figure 1c), in agreement with earlier conjectures [*Kärcher et al.*, 1996]. In the 0.26 g S / kg fuel case, $n_i = 1.1 \times 10^4$ cm^{-3} ice particles are present in the ATTAS plume at a plume age of 1 s, leading to a clearly visible contrail, as observed. At lower temperatures and similar sulfur content, more ice particles are formed (6.5×10^4 cm^{-3}; see dotted-dashed curve). An additional increase of sulfur leads to even more ice particles (1.5×10^5 cm^{-3}; see short-dashed curve). The correspondingly increasing ζ(hom) values in Table 1 show that freezing of volatile particles slightly dominates contrail formation in the very high sulfur case at 218 K and is almost equally important as soot-induced freezing in the low-sulfur case. This goes along with increasing abundances of volatiles in the CN size range ($r > 4$ nm) in Table 1 and Figure 1a.

When going from 0.17 g S / kg to 5.5 g/ kg, it can be seen, by considering the product $n_i\zeta$(hom) from Table 1, that relatively more volatile droplets stay liquid although 3 times more droplets freeze homogeneously in absolute numbers. At the same time, the absolute number density of ice with a soot inclusion, $n_i\zeta$(het), increases by nearly a factor 2, yielding the increase in total n_i. Consistent with this picture, the mean radius of the ice particles decreases, and the optical depth of the contrail increases when the sulfur level is enhanced and/or the ambient temperature is lowered.

2.2. Comparisons

Gierens and Schumann [1996] explained the visible difference of the colors of both contrails by a possible shift in the mean radius of the ice particles from about 0.75 μm and 0.35 μm in the low and very high sulfur cases during SULFUR 2. In our simulation we observe a less pronounced shift from 0.54 μm to 0.45 μm for the contrail ice particles, yielding the same tendency. Estimates of the optical depths made by *Gierens and Schumann* [1996] are also in fair agreement with the calculations that give the range 0.7 − 1.3 (see Table 1). A comparison with the CN data observed at $t = 20$ s is given at the end of this section.

Thus our simulations support the observed color differences between low and very high sulfur contrails. However, the interpretation suggested by the present analysis is different. Whereas Gierens and Schumann, neglecting the volatile aerosols, have speculated that an increased number of soot particles caused freezing when going from low to very high sulfur levels, we have shown that a combination of heterogeneous freezing with additional homogeneous freezing is consistent with the observations. The simulations confirm the conjecture of *Schumann et al.* [1996] that an increase of the FSC leads to a faster growth of the soot coatings due to enhanced uptake of H_2SO_4 (see Figure 1b). They also show that increasing the sulfur level leads to an enhanced production and growth of volatile aerosols.

There is a problem with contrail formation in the 0.002 g S / kg case at 223 K. The ice particles (solid curve) shown in Figure 1c and the τ values in Table 1 for this case show that the model contrail was invisible. This is because the initial ice particle number density stays below the threshold value $n_i^{th} \simeq 10^4\,cm^{-3}$ that we have derived from a visibility analysis based on the SULFUR 1 observations [*Kärcher et al.*, 1996]. The optical depths of the other aerosol components remained too small to be relevant in this case, because the plume was only very slightly and shortly above water saturation. (Note that even less particles would become large enough to freeze if the model would be free of numerical diffusion.) All other cases can well be modeled with the prescribed contact angle $\vartheta = 110°$, as noted above. Decreasing ϑ from 110° to, for example, 70° produces a visible contrail also in the very low sulfur case as observed during SULFUR 1. However, with this choice of ϑ the model cannot reproduce the SULFUR 2 observations, because then soot exclusively dominates the freezing. Most soot particles are transformed into ice already for 0.17 g S / kg and quickly take up the available H_2O, leaving no room for an increase in the ice mass at higher sulfur levels. Increasing ϑ to values above 110° in the calculations does not reproduce the SULFUR 1 observation at average sulfur content (0.26 g S / kg), because then the simulated contrail is invisible.

A likely explanation to remedy this model insufficiency to explain freezing at (very) low ($\lesssim$ 10 ppmM) sulfur levels at threshold temperatures is to postulate a different, sulfur-independent heterogeneous freezing mechanism in such cases (see part 1, Figure 5). For these low fuel sulfur contents, the H_2SO_4/H_2O surface coverage of soot is less than 1 % at the time of contrail formation. The proposed mechanism must work as efficiently as sulfur-induced freezing and must be dominated by sulfur-coating effects above some critical sulfur level. Of course, how much sulfur is necessary to render the pure H_2O coating mechanism unimportant is not well defined.

We have shown recently for the SULFUR 1 case that even a graphite-like, hydrophobic soot surface (without any morphological features or chemical activation) can acquire a partial (20 %) pure water coating at the time of freezing under slightly water-subsaturated plume conditions [*Kärcher et al.*, 1996]. Hence this transient water coating is larger than the H_2SO_4/H_2O coating for low sulfur fuel; see above. The H_2O coating could be enhanced by the presence of charged, large cluster molecules, if their efficiency to be scavenged by soot is greater than for uncharged droplets. (This process is not included in the model.) Also, chemi-ions could directly contribute to the formation of charged soot particles during fuel combustion [e.g., *Bockhorn*, 1994]. Ice may nucleate directly in the liquid water patches on the soot surface, without the freezing point suppression, and hence, sulfur dependence, as in an H_2SO_4/H_2O solution.

However, it can be excluded that the contrails during SULFUR 1 became visible when only ice saturation was reached in the plume [*Busen and Schumann*, 1995; *Schumann*, 1996a], in agreement with other threshold observations [*Jensen et al.*, 1998]. Therefore freezing in the pure water layer must still be characterized by a substantial nucleation barrier due to the imperfect ability of the soot surface to support ice germ formation. In comparison, direct nucleation of ice germs on the "dry" soot surface is probably much less important due to even more stringent microphysical requirements.

It will be difficult to decide experimentally whether a soot particle caused freezing or whether soot was scavenged by a contrail ice particle that formed from homogeneous freezing. The latter is expected to be an efficient process in persistent contrails (part 1, Figure 2). There is indeed observational evidence for exhaust soot and ice interaction from in situ measurements in contrails at estimated plume ages around 40 s [*Ström and Ohlsson*, 1998]. Their finding that ice crystals in the upper part of a contrail can contain a larger concentration of absorbing material (presumably soot) compared to the lower part may be indicative of scavenging of soot that did not initiate freezing. To interpret such observations, calculations of ice microphysics coupled to a three-dimensional dynamical model for the wake turbulence must be performed.

Finally, we will compare the total CN measurements during SULFUR 2 behind the ATTAS at a plume age of 20 ± 1.5 s [*Schumann et al.*, 1996] with the model results. For the low and very high sulfur cases, cumulative CN number densities, $n_>$, have been measured for all particles with radii $r > 3.5$ nm and $r > 9$ nm, respectively. In Figure 2 we plot the time evolution of $n_>$ as a sum over all particle types for $r > 4$ nm and $r > 10$ nm as solid lines without and with circles, the cumulative number density of volatile aerosols with > 4 nm only as dotted-dashed lines, and the total number density of ice particles as long-dashed lines. Figures 2a and 2b show the low and very high sulfur case, respectively. Also shown are the measured values for total CN concentrations as squares (diamonds) for $r > 3.5$ nm ($r > 9$ nm).

First we note that the values for $n_d^>$ and n_i at 1 s are consistent with those given in Table 1. There are two reasons for the drop in $n_d^>$ both in Figures 2a and 2b between 0.1–0.2 s. First, part of the volatiles have been activated into nearly pure water droplets and froze homogeneously; see R values in Table 1. Second, the concomitant depletion of H_2O causes the smallest droplets to evaporate excess H_2O, forcing them to shrink. We recall from part 1 that the critical size above which the droplets can overcome the Kelvin barrier for water uptake under contrail formation conditions ranges between a few nm up to 20 nm, depending on the maximum water supersaturation reached in the plume.

Both the number density of all particles greater than 4 nm and greater than 10 nm radius increase with increasing sulfur level, compare the solid lines in Figures

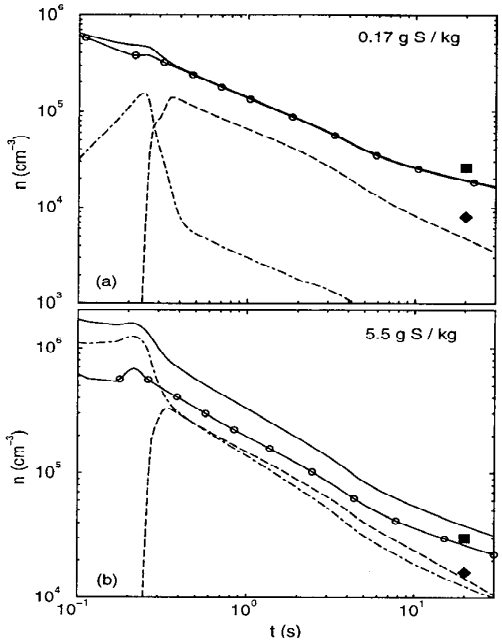

Figure 2. Simulated number densities of all particles with radii $r > 4\,\mathrm{nm}$ (solid lines) and $r > 10\,\mathrm{nm}$ (solid lines with circles), of volatile aerosols only with $r > 4\,\mathrm{nm}$ (dotted-dashed lines), and of all ice particles (dashed lines) in the ATTAS plume during SULFUR 2. The squares and diamonds denote the measured abundances of total CN particles with $r > 3.5\,\mathrm{nm}$ and $r > 9\,\mathrm{nm}$, respectively, at a plume age of 20 s in the (a) low and (b) very high fuel sulfur case.

2a and 2b. This is consistent with the observations, although a difference in the ultrafine size range between 4 nm and 10 nm is only seen in the 5.5 g S / kg case in the model. The inability of the model to resolve this difference for low fuel sulfur levels may well be related to our simplified parameterization of plume ionization microphysics and/or due to numerical diffusion affecting the particle growth equations.

This comparison clearly supports the view that sulfur emissions exert an observable impact on volatile aerosol and contrail formation. The model slightly overestimates the observed CN concentrations, except $n_d(r > 4\,\mathrm{nm})$ for 0.17 g S / kg. We believe that a more detailed comparison is hampered by uncertainties introduced by the few samplings in the spatially inhomogeneous wake during the plume crossings. The sulfur impact on CN formation in aircraft plumes is further substantiated in section 4.1.

3. Sensitivity Studies and Implications From Other Contrail Observations

3.1. Contrail Formation Thresholds

Until recently, it was not clear if contrails only form when the relative humidity in the plume exceeds liquid water saturation, as assumed in the thermodynamic theory of contrail formation. A sufficient number of ice particles might also nucleate well above ice but below water saturation, just as in cirrus clouds. Various plume observations now becoming available convincingly favor the former assumption, indicating the lack of suitable ice nuclei in the exhaust.

Figure 3 summarizes contrail observations behind various airliners from different airborne missions, as

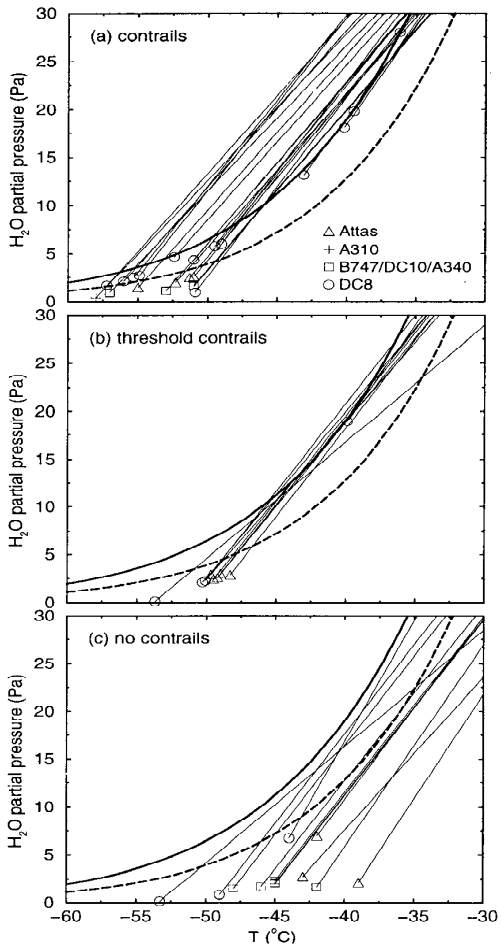

Figure 3. Contrail observations at (a) $T_a < T_{th}$ and (b) $T_a \simeq T_{th}$, and (c) cases where no contrails were observed ($T_a > T_{th}$) in a H_2O vapor pressure versus temperature diagram. The open symbols denote ambient conditions during the different observations. The thick solid and dashed lines are the equilibrium saturation vapor pressures of H_2O. The thin lines are mixing lines, the gradients of which depend on the H_2O emission index, the overall propulsion efficiency, the heat released by fuel combustion, and the ambient pressure. Contrails only form when liquid saturation with respect to water is reached at some point in the plume. Observations were made during the SULFUR missions (triangles), POLINAT (squares), SUCCESS (circles), and behind an A 310 (plus).

given in the legend. The thick solid and dashed lines in each figure part are the saturation vapor pressures over liquid water and ice, respectively. The thin lines depict the evolution of H_2O in terms of vapor pressures versus plume temperature during cooling, assuming isobaric mixing of the exhaust gases with ambient air [*Schumann*, 1996b]. Each of them ends with an open symbol at the measured ambient humidities and temperatures for each observation.

All threshold cases scatter around the liquid saturation threshold (Figure 3b), showing that contrails form as soon as the dashed tangents touch or cross (Figure 3a) the solid line. The plumes stayed below water saturation in all cases where no contrails were observed (Figure 3c). It cannot be excluded that ice still nucleated in the plume. If this occurred, the number of ice particles was too small to make them visible. We note that one contrail was observed at an unusually high temperature, where the ambient air was very near liquid saturation; see the top right-hand open circle in Figure 3a. We will investigate this case in more detail in section 3.4.

3.2. Variations of Ambient Temperature and Fuel Sulfur Content

Our analyses of the contrail observations in section 2.2 suggest that soot initiates contrail formation at and up to about 1 K below threshold temperatures, typically within one wingspan behind the aircraft. For lower temperatures, homogeneous freezing takes over the dominant part. The detailed partitioning between homogeneous and heterogeneous freezing (ratio $R = n_i(\text{hom})/n_i(\text{het})$) depends mainly on the conversion rate of fuel sulfur to H_2SO_4, the presence of chemi-ions, and the plume mixing rate.

We want to use our code to explore implications of this picture when some key parameters are varied. We show results for a B 747, being representative for other large airplanes, that confirm the findings from the last section which were derived from observations in the plume of the much smaller ATTAS aircraft.

In Figure 4 we plot the total number density of ice particles, n_i (circles), the ratio R (squares), and the average radius of the ice particle size distribution $\bar{r}_i$ (diamonds) as a function of the ambient temperature T_a. The calculations were perfomed for a B 747 flying at $p_a = 216$ hPa and RH = 50 %, with 5 % (95 %) of the sulfur molecules exiting the engines as SO_3 (SO_2). Exhaust soot was assumed to be distributed lognormally, with exit plane concentration 2.5×10^6 cm^{-3}, mode radius 20 nm and geometric standard deviation 1.8. The corresponding integral quantities (0.24 g soot or 10^{15} soot particles per kg fuel) are reasonable, but we emphasize that the assumed soot distribution is only an educated guess because it has never been measured in situ. Background aerosols are neglected, for simplicity.

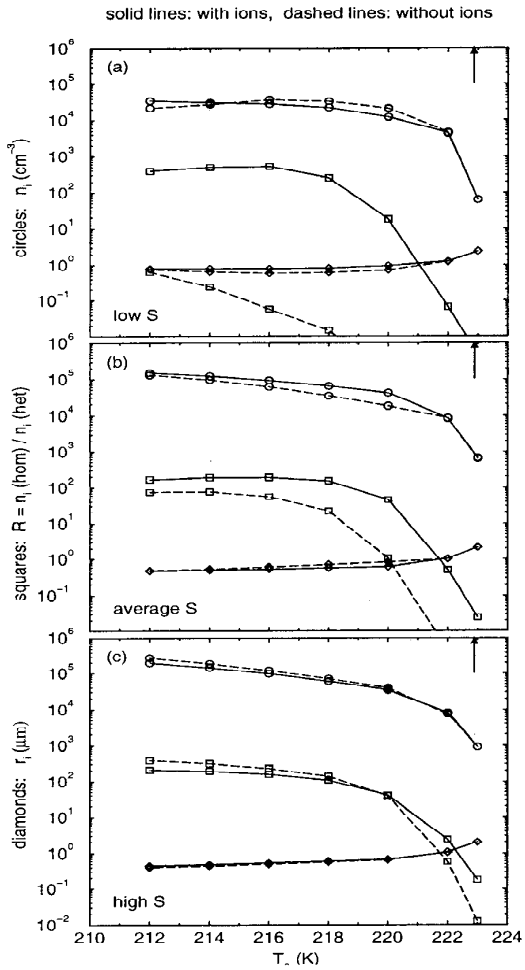

Figure 4. Contrail formation parameters for a B747 at 216 hPa and RH=50 % for different ambient temperatures T_a and for different FSCs after freezing. (a) Low: 0.05 g S / kg fuel; (b) average: 0.5 g S/kg; (c) high: 2.5 g S/kg. Shown are the total number density of ice particles (n_i, circles), the number density ratio R of homogeneously versus heterogeneously frozen aerosols ($n_i(\text{hom})/n_i(\text{het})$, squares), and the mean radii of the ice particles ($\bar{r}_i$, diamonds) at a plume age of 3 s. Calculations assumed an exit plane mixing ratio $[SO_3]/[SO_x] = 0.05$, including (excluding) the effects of chemi-ions depicted as solid (dashed) lines. The arrows mark the thermodynamic threshold temperature 222.9 K for contrail formation.

The Figures 4a, 4b, 4c assume low (0.05 g S/kg fuel), average (0.5 g/kg), and high (2.5 g/kg) FSC, respectively. Solid (dashed) lines represent results from simulations including (excluding) ion effects. Results are plotted at $t = 3$ s, when the plume approached ice saturation after freezing and ice particle growth ceased.

The guessed number-based soot emission index for the B 747 is in good general agreement with measured

nonvolatile CN in aircraft plumes, and the mass-based value lies within the broad range of data that can be found in the literature. However, to effectively constrain the calculations, knowledge of emission indices alone is not sufficient, and further details of the size distribution (mean radius and width) have to be prescribed. These parameters are available from measurements only in rare cases, as for the ATTAS. Observations for the ATTAS revealed that the soot emission index does not, or only weakly, depend on the fuel sulfur content (*Petzold et al.*, manuscript in review, 1998), so we keep the given soot parameters constant in all our simulations for the B 747.

The arrows mark the thermodynamic threshold temperature $T_{\rm th} = 222.9\,{\rm K}$ for this aircraft and ambient parameters, calculated using an overall propulsion efficiency of 0.3. The simulations generally confirm that for $T_{\rm a} > T_{\rm th}$ visible contrails do not form, as can be seen in the steep decrease of $n_{\rm i}$ when $T_{\rm a}$ approaches $T_{\rm th}$, although some ice particles do nucleate just slightly above $T_{\rm th}$. The simulations are also in excellent agreement with the visibility analysis based on the SULFUR 1 observations, as mentioned in section 2.2.

Soot particles acquire (partial) liquid coatings in the nascent plume by adsorption and scavenging of gaseous oxidized sulfur and H_2SO_4/H_2O droplets. In this liquid layer, water ice nucleates heterogeneously when the plume approaches water saturation. At threshold conditions, homogeneous freezing cannot compete with heterogeneous freezing (due to the difference in the mean particle size of volatile and soot particles), eliminating the sulfur dependence in such cases. At $T_{\rm a} \simeq 222.5\,{\rm K}$ and for average and high-sulfur levels shown in Figures 4b and 4c, the $n_{\rm i}$ values are close to the threshold $n_{\rm i}^{\rm th} \simeq 10^4\,{\rm cm}^{-3}$, leading to visibile contrails. For low sulfur levels, $n_{\rm i} < n_{\rm i}^{\rm th}$ (Figure 4a), obviously soot and sulfur interaction alone (and homogeneous freezing as well) is insufficient to form ice particles, for which we argued that freezing in a pure liquid water coating on soot may be responsible for ice formation. For decreasing temperatures, ice particle concentrations increase progressively. This increase saturates early for low sulfur levels. Relatively more ice particles nucleate for larger fuel sulfur levels, in which case more particles are activated into water droplets prior to freezing.

One might expect a much larger change in contrail optical properties when homogeneous freezing dominates, because at some point the number of volatiles available for freezing becomes much larger than the number of ice particles $n_{\rm i}^{\rm th}$ required for visibility (see also Figure 1a, short-dashed line). However, freezing in young contrails is a self-limiting process, and H_2O depletion from the gas phase slows further nucleation for $n_{\rm i} \gtrsim 10\,n_{\rm i}^{\rm th}$.

The corresponding variations in the mean size $\bar{r}_{\rm i}$ of the ice particles are moderate for all sulfur levels (see also Figure 1c). This is because the ice mass in the young contrail is exclusively determined by the exhaust water vapor mass and $n_{\rm i}$, i.e., $\bar{r}_{\rm i} \propto n_{\rm i}^{1/3}$. However, in agreement with Figure 1c, $\bar{r}_{\rm i}$ values at a given temperature decrease by a factor of two when going from low to high fuel sulfur levels (assuming a constant fraction of $[SO_3]/[SO_x]$ at emission). In general, $n_{\rm i} \simeq 10^4 - 2 \times 10^5\,{\rm cm}^{-3}$ and $\bar{r}_{\rm i} \simeq 0.4 - 1\,\mu{\rm m}$.

We finally discuss the R values shown in Figure 4. Values of R greater (smaller) than unity indicate that more (less) ice particles formed by homogeneous freezing than by soot-induced heterogeneous freezing. At the formation threshold (see arrows) we see $R < 1$, underlining the important role of soot in contrail formation in such cases, especially for low sulfur levels. The contrails are invisible in the latter case, indicating that homogeneous freezing alone is not the key contrail-forming mechanism. Invoking a second freezing mode on soot as discussed in section 2.3 may easily lead to more and visible ice particles.

Decreasing the temperature (and/or increasing the available sulfur level) progressively favors homogeneous freezing of freshly nucleated volatile droplets over soot-induced freezing, as indicated by rising values of R in Figures 4a-4c. This is because the soot surface area does not increase (because it shows no dependence on $T_{\rm a}$ and FSC), whereas the number density of volatiles that grew beyond the size where they can freeze homogeneously does increase.

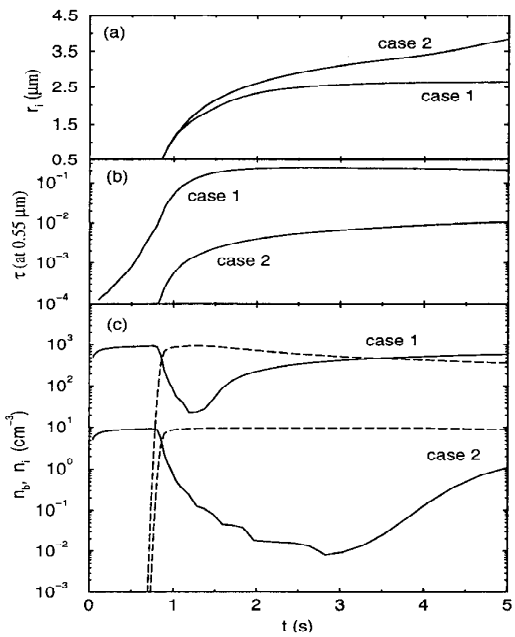

Figure 5. Contrail formation in the B 747 plume at 221 K ($T_{\rm th} - T_{\rm a} \simeq 2\,{\rm K}$) in the absence of soot and sulfur emissions. Shown are (a) the average radii of the ice particles, (b) the contrail's optical depth, and (c) the number densities of entrained background aerosols and nucleated ice particles versus plume age. Cases 1/2 assume $n_b = 1000/10\,{\rm cm}^{-3}$.

In the high-sulfur case, values for $n_i, \bar{r}_i$, and R in Figure 4c are similar, whether chemi-ions are included or not. This is because the growth and coagulation rates in both calculations are so large that a possible ion effect on freezing cannot be distinguished. In contrast, including chemi-ion emissions for average and low FSCs leads to enhanced homogeneous freezing, especially in the low-sulfur case, causing much higher R values in Figures 4a and 4b when ion effects are considered compared to calculations when they are neglected. This is because chemi-ions lead to a bimodal size distribution of the new volatile aerosols, one slowly growing mode located at sizes below 1 nm, and the other, faster growing mode at sizes well above 1 nm [*Yu and Turco*, 1997; part 1, Figure 2]. Only the largest freshly nucleated volatile aerosols overcome the Kelvin barrier, thus efficiently condense H_2O and freeze [*Kärcher et al.*, 1995].

Numerical diffusion does not affect these results but merely causes a tiny shift (< 0.1 s) of the onset of ice nucleation toward earlier plume ages and slightly overestimates the numerical R values. The discussion about the temperature dependence of contrail properties is strongly supported by lidar observations of contrails. *Freudenthaler et al.* [1996] derived depolarization data from lidar measurements for contrails nucleated at ambient temperatures from 225 K to 210 K. They found a decrease in the radii of contrail ice particles with decreasing temperature. This behavior is qualitatively consistent with the results shown in Figure 4 and increases confidence in the present model results.

3.3. Contrails Formed Without Soot and Sulfur Emissions

What would happen if the number density of soot particles emitted by jet aircraft is strongly reduced (i.e., by two orders of magnitude), or if the engines emit no soot particles at all ? From the preceding interpretation of Figure 4 it is obvious that contrails would still form in all cases, where the ratio R exceeds unity, because then, homogeneous freezing is found to dominate ice formation anyway. Because $R < 1$ only in the vicinity of T_{th}, contrail onset is likely shifted to slightly lower temperatures without soot emissions. According to our simulations, number density, average radius, and optical depth of the contrails do not change significantly. Thus reducing the soot production efficiency of jet engines does still lead to the formation of contrails. Contrails would then form on volatile aerosols, starting at slightly lower threshold temperatures. However, reducing soot emissions avoids the potential danger that these particles affect cirrus cloud formation and evolution.

What would happen if the average FSC is substantially lowered, or perhaps the kerosene is desulfurized, but the soot emissions are kept as they are ? Soot activation by sulfur is suppressed in this case, but it seems very likely that ice still forms heterogeneously in a pure liquid water coating. More and more soot particles will freeze with increasing difference ($T_{th} - T_a$), and the variation in contrail parameters will be similar to those discussed in Figure 4. This view is strongly supported by the observations reported by *Busen and Schumann* [1995].

Finally, would contrails still form without soot and sulfur emissions ? The answer is yes, but the contrail parameters will depend on the highly variable microphysical parameters of the background aerosols that are entrained into the plume and freeze in this case.

To support this statement, we have performed calculations for the B 747 with average FSC and using the same initialization as given in section 3.2. We show a calculation at 221 K (~ 2 K below T_{th}). The simulations include two lognormal size distributions for the background aerosols (assumed to be H_2SO_4/H_2O droplets): case 1 with total number density $1000\,cm^{-3}$ and case 2 with $10\,cm^{-3}$. The mode radius and modal width are $0.1\,\mu m$ and 1.8, respectively, in both cases. Figure 5 depicts (a) the mean radius $\bar{r}_i$ of the ice particles, (b) the contrail's optical depth τ, and (c) the number density of background aerosols, n_b, and contrail ice particles, n_i, as a function of plume age.

Clearly, visible contrails with comparable mean sizes form by homogeneous freezing of ambient aerosols in both cases. Background aerosols are entrained into the plume within about 1 s and subsequently freeze, causing the rapid increase in n_i and τ. The liquid aerosol "hole" in the plume is filled soon after freezing nucleation ceased. The maximum supersaturation achieved in the plume is higher in case 2 because fewer ice particles are formed. Thus the time needed to deplete the available H_2O is correspondingly longer, and freezing extends to greater plume ages than in case 1. Hence the crystals in case 2 become larger because the same amount of H_2O vapor distributes over fewer particles. For the same reason, the optical depths of both contrails differ by a factor 20 at $t = 5$ s. Note that the ice particle radius in case 2 is still increasing rapidly at the end of the simulation, indicating that the small number of ice particles cannot sufficiently deplete the H_2O. Of course, this growth will be modified in other parts of the wake, depending on the mixing histories along the different flow streamlines.

Sizes are markedly larger and optical depths can be considerably lower than in contrails formed in the presence of soot and sulfur emissions. This situation should be similar in the case of contrails formed by liquid hydrogen engines [*Schumann*, 1996b]. One might think that this causes faster precipitation of the contrails due to greater sedimentation velocities, thus reducing their potential radiative impact. However, only some ice particles in persistent contrails grow large enough (e.g., $> 10 - 50\,\mu m$, see *Minnis et al.*, [1998]) and can potentially fall out of the layer in which they were generated. Since the growth of ice crystals in persistent contrails is controlled by the evolution of the ambient ice supersaturation (which is in turn influenced by the number density of contrail ice particles), this growth should be

insensitive to the comparatively small initial size of the crystals shown in Figure 5a.

3.4. Possible Role of Entrained Cirrus Ice Crystals and Emitted Metal Particles

According to thermodynamic theory the formation of contrails should be suppressed above temperatures of about 223 – 228 K at flight levels above ~ 300 hPa. However, during the SUCCESS mission, a contrail was observed behind the DC-8 aircraft at $T_a = 237$ K (case 5 in the work of *Jensen et al.* [1998]; see also Figure 2a). The ambient air was just below liquid water saturation. We argue that the presence of diffuse cirrus may have been responsible for the formation of these "warm" contrails. Cirrus ice crystals could sublimate in the warm plume and the additional water vapor adds to the H_2O mass emitted by the engines. The patches of the diffuse cirrus observed during SUCCESS contained ice particles with a mass-averaged radius of about 175 μm and number density about 10 ℓ^{-1} according to measurements with the optical array (2D-C) probe. Crystals with sizes lower than 50 – 100 μm could not be detected by this instrument.

Knowledge about the microphysical properties of contrails that form in a strongly ice-supersaturated region or within thin cirrus sheets is important, because these contrails are persistent and will preferably develop into cirrus decks with great spatial extent, and hence potentially large radiative impact.

To study the characteristics of "warm" contrails, we initialized an Airbus A 310 engine/plume configuration at $p_a = 367$ hPa, $T_a = 237$ K, and RH = 99 %, according to the SUCCESS measurements. Under these conditions the threshold formation temperature is $T_{th} = 234.5$ K. In the calculation, the ambient cirrus cloud within which the contrail forms is represented as a monodisperse size mode with mean radius and number density as given above. The PCASP measurements of the dried aerosol in the Airbus plume during SULFUR 4 (flight on March 13, 1996) allows to estimate the soot properties. It is characterized by a lognormal distribution with initial number density 3.3×10^7 cm^{-3}, geometric mean radius 20 nm, and geometric standard deviation 1.7. We assume an average sulfur content of 0.3 g S per kg fuel, an exit plane ratio $[SO_3]/[SO_x] = 0.02$, and include chemi-ion emissions in the calculation. With the H_2O emission index of 1.25 kg H_2O per kg fuel (corresponding to an exit plane volume mixing ratio 27,280 ppm), the plume does not reach water saturation but slowly approaches the ambient relative humidity.

Ice crystals drawn into the jet engine may sublimate in the warm core and bypass engine flow, releasing additional H_2O. Applying the Schmidt-Appleman criterion, we estimate that the H_2O emission index must be increased by a factor > 1.58 in order to push T_{th} above the ambient value 237 K. The cirrus ice water content measured during SUCCESS corresponds to additional 1600 ppm H_2O at the exit plane under core flow conditions (temperature 564 K). However, the relative increase of plume H_2O due to evaporating cirrus ice crystals could be larger in the bypass region of the jet plume. Sublimation of crystals that are entrained later into the plume could also affect the plume humidity. To test this, we entrained a monodisperse crystal mode (175 μm) into the plume and let them sublimate. We found that this is too slow to enhance the plume H_2O due to the assumed large crystal sizes and correspondingly long sublimation timescales. However, the actual crystal size distribution could well extend to smaller sizes, and already partial sublimation could then contribute to H_2O.

It is not easy to take these effects into account in a box model that gives only results that are representative for the core flow. However, we estimate that the entrained H_2O mass of the evaporating cirrus crystals can be comparable or even greater than the emitted H_2O mass at the point in the bypass region of the wake where freezing sets in (accounting for dilution of emitted H_2O). Since we cannot model this effect, we simply assume a corresponding increase of the H_2O emission index in the jet core by about a factor 1.5. We will treat two cases: case 1 assumes an effective H_2O emission of 40,000 ppm in the box model as a reasonable upper limit, and case 2 assumes the increase 1600 ppm of exhaust H_2O, as noted above (giving 28,880 ppm), as a lower limit. In case 1 the maximum plume relative humidity is 102 % and case 2 leads to a peak value of 98.5 % (including the H_2O depletion due to the growing ice crystals).

Figures 6a, 6b, and 6c show the average ice particle radius, $\bar{r}_i$, the contrail's optical depth at 0.55 μm, τ, and total number density n_i of ice particles, respectively, versus plume age for both cases (cases 1/2 as a solid/dashed line). As before, we define the values $\bar{r}_i$ as the number density average over the total (contrail and cirrus) ice size distribution. The average radius of the contrail embedded in an existing cirrus cloud starts at 175 μm, the radius of the entrained, monodisperse crystals. In case 1 (see solid lines), $\bar{r}_i$ drops rapidly to 36 μm at $t = 9$ s as more, but smaller ice particles nucleate in the contrail and add to the entrained ice particle abundance. The radius then increases to 40 μm after 30 s. Note that n_i in Figure 6c levels off after $t = 10$ s, i.e., during the vortex regime. The transient suppression of mixing which is typical for this period of wake evolution causes a small increase in supersaturation which in turn leads to additional freezing. The optical depth shown in Figure 6b increases to a peak value of 0.1 at 2.5 s, leading to a clearly visible contrail. Inspection of the contributions of the different particle types at $t = 30$ s reveals that coated exhaust soot contributes most to the optical depth ($\tau_d = 0.002$ and $\tau_s = 0.012$ compared to $\tau_i = 0.004$).

In case 2 (see dashed lines), the perturbation of the entrained ice spectrum is hardly visible in Figure 6 because the number of new contrail ice particles is much

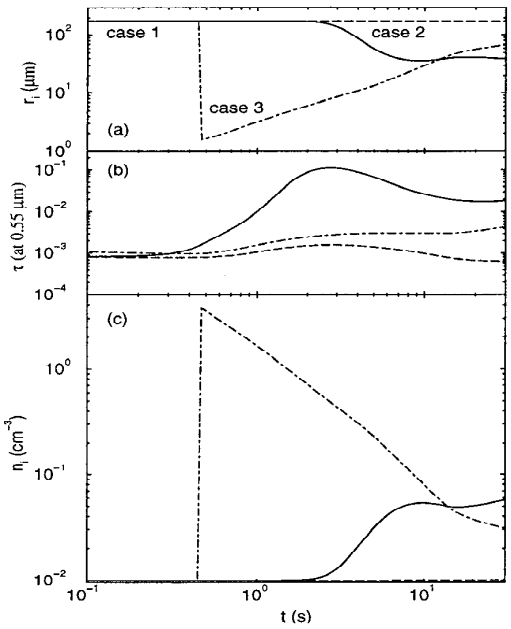

Figure 6. Visible "warm" contrails nucleated in an A 310 exhaust plume embedded in an ambient, diffuse cirrus cloud. Shown are (a) the average radius and (b) the total number density of both contrail and cirrus ice particles versus plume age. In cases 1/2 the plume was slightly supersaturated/subsaturated with respect to liquid water. Case 3 is similar to case 2 but included the emission of metal particles which are assumed to be perfect IN. As in Figure 5, model-derived optical depths are only estimates.

smaller up to $t = 30$ s than in case 1: slightly less than $0.01\,\ell^{-1}$ ice particles with radii around 15 μm nucleated after 30 s, with increasing tendency. This contrail is predicted to stay invisible, despite the transient increase of τ between 2 and 6 s caused by soot.

In recent plume measurements, *Petzold et al.* [1998] characterized metal particles that obviously constitute a subset of the emitted, nonvolatile exhaust particles. With typical radii of the order of 1 μm their abundance at emission is much lower compared to soot but comparable in terms of total mass. With $r_s = 20$ nm, typical abundances of metal particles at the nozzle exit plane of the jet engines should be $(20\,\text{nm}/1\,\mu\text{m})^3 = 8 \times 10^{-6}$ times lower than for soot, i.e., in the range $10 - 100\,\text{cm}^{-3}$. We point out that this choice for the emission index of metal particles is only an educated guess, because no systematic studies about the variability of metal emissions are available to date.

Depending on their ice-nucleating ability, metal particles may contribute to the formation of large ($> 1\,\mu$m) contrail ice particles due to their initial size, although they will certainly not form the bulk of the ice water content in contrails formed at $T_a < T_{th}$. However, if the metal particles are more efficient ice nuclei (IN) than exhaust soot, they may be responsible for the nucleation of ice particles that could form when the plume gets ice but not water supersaturated. The dashed-dotted lines in Figure 6 (case 3) are obtained from a simulation similar to case 2 but with added monodisperse metal particle emissions (radius 1 μm, exit plane number density $30\,\text{cm}^{-3}$).

To maximize their effect on ice nucleation, we assumed them to be perfect IN, that is, we prescribe a contact angle of 0° and a pure water coating to calculate the heterogeneous freezing rate. Clearly, the metals can strongly modify the contrail properties under these assumptions. As soon as ice supersaturation is achieved in the plume, nearly all of them freeze and accumulate exhaust and entrained water vapor. This can be seen in Figures 6a and 6c by the decrease of $\bar{r}_i$ to about the initial size of the metal particles and the steep increase of n_i due to freezing of almost all of them. In this case, these new ice crystals make up the total optical depth $\tau \simeq \tau_i = 0.004$ at 30 s, with increasing tendency (Figure 6b). However, the small ice particles with the metal cores rapidly dilute, which shifts the number density-averaged radius in Figure 6a farther toward the ambient cirrus particle radius later in the plume (60 μm at $t = 30$ s). This is contrast to case 1, where more and more volatile plume aerosols are progressively activated and freeze with increasing plume age, thus counteracting dilution.

Volatile plume aerosols dominated ice nucleation by homogeneous freezing in case 1 ($\zeta(\text{hom}) = 0.99$, $\zeta(\text{het}) = 0.01$). The fraction of ice crystals with soot inclusions in case 2 is much larger than in case 1 ($\zeta(\text{hom}) = 0.03$, $\zeta(\text{het}) = 0.97$). In case 3, virtually all ice nucleated on the metal particles, whose freezing and growth suppressed freezing of other plume aerosol components up to the end of the simulation. However, because the freezing properties of soot and metal particles are not well known and because of uncertainties in the prediction of the volatile nucleation mode aerosols, the detailed impact of aircraft exhaust aerosols upon the formation of these "warm" contrails remains uncertain. Interstitial background aerosol, which we have neglected in the simulations, may also become activated in the plume and contribute to the ice mass in contrails [*Gierens and Ström*, 1998].

In any case, it is interesting to see that the microphysical properties of contrails that formed within cirrus clouds under strong ice supersaturations are very different from contrails formed in clear, drier air. This is because the ice growth in a persistent contrail is controlled by ambient water vapor rather than by the limited amount of exhaust H_2O, causing rapid increase of the ice particle size to several 10 μm within only minutes. To generate persistent, "warm" contrails, the plume does not neccessarily need to experience water supersaturation. Further, the simulations suggest that the size distribution and hence the radiative properties of natural cirrus clouds can be modified by aircraft ex-

haust aerosols on timescales of the order of a few hours. Of course, more detailed conclusions require modeling efforts that go beyond the capabilities of this box model.

4. Observations During SULFUR 4 and 5

More systematic in situ measurements of the microphysical properties of aircraft-produced aerosols and their dependence on the fuel sulfur content have been made during the recent SULFUR 4 and 5 missions in 1996 and 1997 [*Petzold et al.*, 1997; *Busen et al.*, 1997].

4.1. Plume Aerosols in the Ultrafine Size Range

We concentrate on the SULFUR 4 ATTAS flight on March 15 at $p_a = 287.4$ hPa and $T_a = 220.8$ K and RH = 40 %. The jet engines of the ATTAS carried fuel with 6 ppmm and 2700 ppmm sulfur mass content. In both cases, short-lived contrails were produced by the aircraft that started to evaporate at the end of the jet regime (after $t \simeq 10$ s). The liquid saturation threshold temperature was $T_{th} = 223.1$ K, or $T_a - T_{th} = 2.3$ K. Ambient aerosols have also been measured during the flights and are taken into account in the simulations.

Table 2 lists the results from the observations [*Petzold et al.*, 1997] and from our model. We compare the ultrafine CN fraction (UCN) as defined in the table caption and the total number density of plume aerosols with $r > 5$ nm for different assumptions regarding emissions of SO_3 and chemi-ions n_{ci}. In addition to the total CN numbers, the UCN values yield information about the distribution of volatile plume aerosols in the radius range between 4 nm and 10 nm compared to the total aerosol abundance. (We recall that the mean radius of the ATTAS soot particles is 25 nm; most of them are not within the UCN range.) Because of our simplified treatment of chemi-ion microphysics and because we do not introduce the ions as a separate aerosol class in our model, we cannot compare the results to observed data whenever the number density of H_2SO_4 molecules in the plume does not surpass the prescribed number density of emitted chemi-ions. This holds for the low-sulfur case (dashes in Table 2).

The far-field observations show significant increases in the UCN fraction over background levels (the latter were measured to be below 10 %). The increase is more pronounced in the high-sulfur (20 – 40 %) than in the low-sulfur case (40 – 60 %). This distinct dependence of nuclei mode particles to the FSC strongly suggests that volatile aerosol production in aircraft plumes is linked to homogenous nucleation and growth of H_2SO_4 and H_2O. The far-field observations also show an increase by

Table 2. Simulation Results for the Ultrafine Condensation Nuclei (UCN) Fraction and the Total Number Density of Aerosols With Radii > 5 nm, $n(r > 5\,\text{nm})$, in Comparison With Data From in Situ Observations Made During the SULFUR 4 Campaign Behind the ATTAS Aircraft.

	UCN, %[a]			$n(r > 5\,\text{nm})$, $\times 10^4\,\text{cm}^{-3}$		
chemi-ions, cm^{-3}	0	4 (+7)	1 (+8)	0	4 (+7)	1 (+8)
Observations[b]						
Near field		no data			2 – 8 / 2 – 8	
Far field		20 – 40 / 40 – 60			0.5 – 1.5 / 1 – 3	
Simulations[c]						
Near field	1 / 72	— / 8	— / 17	8.1 / 8.2	— / 8.6	— / 8.1
Far field	1 / 76	— / 9	— / 17	2.0 / 1.8	— / 1.8	— / 1.8
Simulations[d]						
Near field	1 / 97	— / 32	— / 47	8.1 / 12	— / 8.5	— / 9.1
Far field	1.2 / 97	— / 32	— / 47	2.0 / 2.8	— / 1.9	— / 2.1
Simulations[e]						
Near field	1.2 / 99	— / 50	— / 65	8.1 / 23	— / 9.3	— / 11
Far field	1.2 / 99	— / 50	— / 65	2.0 / 6.2	— / 2.2	— / 2.6

Data are listed for the low and high fuel sulfur cases (0.006 and 2.7 g S / kg) in the form low-S data / high-S data. Simulations have been performed for three different initial chemi-ion densities and exit plane ratios $[SO_3]/[SO_x]$ (s), as indicated. Near field (far field) indicates that measurements and simulations are given for a plume age around 1.5 s (11 s), corresponding to a distance 250 m (1800 m) behind the aircraft. A contrail has formed in the ATTAS plume. Read 4 (+7) as 4×10^7.

[a] The UCN fraction is defined by $100 \times [n(r > 4\,\text{nm}) - n(r > 10\,\text{nm})]/n(r > 4\,\text{nm})$.

[b] The observations show a distinct variability between individual measurements in the plume. We indicate the range of observed values. No near-field UCN data are available due to saturation of the CN counter (> 4 nm) and the $n_>$ near field data must be regarded as lower limits.

[c] $s = 0$. In this case, the conversion of fuel sulfur to H_2SO_4 is limited by the available exhaust OH.

[d] $s = 0.02$.

[e] $s = 0.04$.

about a factor of two in the cumulative number density of aerosols with $r > 5$ nm when the sulfur content is enhanced by a factor of 450 in the presence of a contrail. Such a trend is not evident in the near-field data.

In comparison to the far-field data, interpretation of the near-field measurements is hampered by a smaller statistical significance (fewer data points were sampled). More importantly, particle abundances detected by the CN counters were so high that saturation effects and coincidences in the instrument could not be excluded. Also, inhomogeneities in the plume are pronounced that it was difficult to get clear correlations between measurements made with different instruments. Systematic effects cannot be excluded because the measuring aircraft always entered the ATTAS plume from below. For these reasons, no UCN fractions have been derived from the observations and the values $n(r > 5\,\mathrm{nm})$ must be regarded as lower limits.

In the high-sulfur case we calculate UCN fractions ranging between 32 % and 65 % in the far-field for $s = 0.02 - 0.04$ and including chemi-ions, roughly consistent with the observed values 40 – 60 %. If we switch off direct emissions of SO_3, the values 8 – 17 % are too small to explain the observations. If we neglect the effects of chemi-ions on aerosol microphysics, very high UCN fractions 72 – 99 % are predicted by the model, contradicting the observations. For $n_{ci} = 0$, the model predicts values around 1 % for low fuel sulfur level which are well below the measured range 20 – 40 % in this case.

There is a straightforward physical explanation for this behavior. Without chemi-ions the volatile nucleation mode is described by a steep radial size distribution initially located at radii < 1 nm. The spectrum is shifted to larger sizes, initially by condensation and later by coagulation. This shift is not significant in the low-sulfur case, and most of the new aerosols remain small ($r < 1$ nm) and are not detectable by the CN counters at this stage. In the high-sulfur case, the shift is very pronounced, so many of the new aerosols grow beyond the CN detection limit and then even dominate the total particle spectrum. In contrast, the presence of charged particles leads to a bimodal spectrum of volatile particles already at plume ages below 1 s, the ion mode having grown to sizes of a few nanometer. Increasing the sulfur level causes more charged aerosols to grow beyond the CN detection limit (on the expense of the neutral volatiles that stay at smaller sizes), but this effect is limited because there is an upper bound to n_{ci}, which is much smaller than the H_2SO_4 number density for average fuel sulfur levels and s values of the order of a few percent. Although our model results for (very) low FSCs may be affected by numerical diffusion (see also section 4.3), we have checked by varying the bin size increments that this principle picture is robust for average to very high FSCs.

Thus the observed moderate change of UCN levels when going from low to high FSC suggests that chemi-ions control volatile aerosol formation and growth [*Yu and Turco*, 1997; part 1]. Unfortunately, we cannot further check this conclusion in the low sulfur case, as mentioned above. Because the corresponding sulfur level in SULFUR 4 (6 ppmm) is only slightly higher than the very low-sulfur case in SULFUR 1 (compare section 2.1.), we might expect ion effects in the SULFUR 4 low-sulfur case as well.

Prescribing $s = 0.02$ and $n_{ci} = 4 \times 10^7\,\mathrm{cm}^{-3}$ for 2700 ppmm fuel sulfur yields simulated total CN number densities $n(r > 5\,\mathrm{nm})$ which compare well with the far-field observations. Increasing (decreasing) s and n_{ci} tends to overpredict (underpredict) the measured CN values, although the dependencies are much less pronounced than for the ultrafine aerosol fractions.

4.2. FSSP Size Distributions

Radial size distributions of plume aerosols have been measured with the FSSP detecting all particles greater than $D = 300$ nm diameter. We compare the ATTAS high-sulfur case in the far field using $s = 0.02$ and $n_{ci} = 4 \times 10^7\,\mathrm{cm}^{-3}$ as guided by the discussion of the UCN data in the last section. The simulated fractions of ice particles that froze homogeneously, ζ (hom), and, heterogeneously involving soot, ζ (het), are 0.06 and 0.94, respectively. Since we found earlier that the differences in the mean radius and number density of ice particles are not very pronounced when going from low to high sulfur levels with and without ions (see Figure 4), we also compare a far-field simulation of the aerosol spectrum in the low-sulfur case using $s = 0.02$ and $n_{ci} = 0$ with the observations. In this case we find $\zeta(\mathrm{hom}) = 0.007$ and $\zeta(\mathrm{het}) = 0.993$, indicating that again, most ice particles contain soot inclusions.

The sum of the distributions $dn_s/d\log(D)$ (coated soot) and $dn_i/d\log(D)$ (ice particles) is depicted in Figure 7 for 6 ppmm (solid line) and 2700 ppmm (dashed line). Curves with circles are measured distributions.

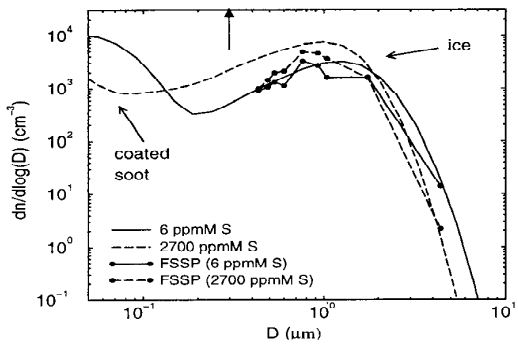

Figure 7. Aerosol size distributions measured with the FSSP in the ATTAS wake at a plume age $t = 11$ s (circles) for two different FSCs (solid line, low; dashed line, high). The corresponding lines without circles are model results and represent the sum of coated soot particles (mostly left of the FSSP detection limit; see arrow) and ice particles.

The vertical arrow points to the lower detection limit of the FSSP, indicating that only ice particles have been measured with this instrument. At 11 s the observations (simulations) show an increase of n_i from $1500\,\mathrm{cm}^{-3}$ ($4400\,\mathrm{cm}^{-3}$) to $2000\,\mathrm{cm}^{-3}$ ($9300\,\mathrm{cm}^{-3}$), accompanied by a decrease of $\bar{D}_i$ from $1.2\,\mu\mathrm{m}$ ($1.22\,\mu\mathrm{m}$) to $1.07\,\mu\mathrm{m}$ ($0.92\,\mu\mathrm{m}$) when the fuel sulfur is increased from 6 ppmm to 2700 ppmm, respectively. These figures translate into a simulated ice water content of $6\,\mathrm{mg\,m}^{-3}$ in both cases, compared to the measured value $\sim 2\,\mathrm{mg\,m}^{-3}$.

The difference in $dn_i/d\log(D)$ between the low- and the high-sulfur case is not very pronounced, as we could have expected from the previous discussion of contrail formation, although the model suggests a somewhat greater sulfur impact. The agreement between calculated and measured far-field spectra is fair. Both observed and calculated spectra exhibit a rapid decrease for diameters $> 4\,\mathrm{nm}$. The tail seen in the small size region ($0.1\,\mu\mathrm{m} < D < 1\,\mu\mathrm{m}$) is indicative of an evaporating ice particle ensemble. However, simulated abundances are a factor 3–4 higher than the measured values. We did not adjust the dilution ratio in the model; changes in the prescribed mixing rates (especially during the transition from the jet to the vortex regime) could explain this discrepancy.

In two single events, FSSP spectra have also been measured in the near field behind the ATTAS [*Petzold et al.*, 1997]. Interestingly, a 2 – 3 times lower number density of larger ice particles, $n_i \simeq 800\,\mathrm{cm}^{-3}$ and $\bar{D}_i \simeq 2\,\mu\mathrm{m}$, has been observed at $t = 1.5\,\mathrm{s}$, suggesting that n_i increases with plume age in the jet regime. Such a behavior is not seen in the simulations. The model predicts a short period where activated plume aerosols undergo a liquid growth stage (activation into nearly pure water droplets) prior to freezing. The production of a large number of ice particles ($n_i > n_i^{\mathrm{th}} \simeq 10^4\,\mathrm{cm}^{-3}$, see section 3.2.) shuts off nucleation typically after $t = 0.5\,\mathrm{s}$. Hereafter, the new ice particles dilute in the spreading wake (n_i decreases with time). Since we cannot exclude that the low number densities of ice at 1.5 s may be caused by saturation effects in the instrument and/or by plume inhomogeneities, we do not further investigate this issue.

4.3. Implications From Other Observations

We summarize the volatile CN abundances measured in young exhaust plumes and study the dependence on FSC and ambient temperature. We may express these abundances in terms of the total number N of aerosol particles per kilogram fuel. Following *Schumann et al.* [1998], N is given by

$$N = \frac{\lambda}{\rho}\frac{n_>(t)}{\mathcal{D}(t)},$$

where λ is the air/fuel ratio at the engine's exit plane, ρ is the local mass density of air, $n_>$ is the cumulative number density of particles that can be detected by a CN counter, and $\mathcal{D}$ is the plume dilution ratio. The latter can be defined by $A_{\mathrm{exit}}/A(t)$, where $A(t)$ denotes the cross sectional area of the wake at the plume age t. Typical values at the flight levels are $\lambda \simeq 70\,\mathrm{kg}$ air/kg fuel and $\rho \simeq 0.5\,\mathrm{kg/m}^3$, leading to the relationship $N[\#(\mathrm{kg\,fuel})^{-1}] = (1-2) \times 10^8 n_>[\mathrm{cm}^{-3}]/\mathcal{D}$.

If the evolution $n_>(t)$ is exclusively governed by wake dilution at constant temperature, $n_>(t)/\mathcal{D}(t)$, and thus N, is constant and given by the initial values of these quantities. In the case of volatile aerosols the ratio becomes time dependent, because condensation and coagulation cause the fine aerosols of the nucleation mode to surpass the CN detection limit. This type of aerosol dynamics is especially important in the first few seconds after emission, as discussed above (see, for example, Figure 2). In the case of soot we discuss the N values at emission only as upper limits, for simplicity, because we are interested in an order of magnitude comparison with the volatile CN levels. (N(soot) may decrease due to freezing and scavenging by ice particles when contrails form.)

Table 3 lists the approximate particle numbers for the ATTAS as we extracted them from the measurements during SULFUR 2 and 4. Various observations

Table 3. Approximate Number of Volatile Plume Aerosols With $r > 4\,\mathrm{nm}$, N(vol), Extracted From in Situ Measurements During the SULFUR 2 and 4 Field Missions.

Fuel S, g/kg	T_a, K	t, s	$\mathcal{D}$	$n_>$, cm^{-3}	N(vol), # (kg fuel)$^{-1}$
0.006[a]	221	1	1.0 (−2)	8.0 (+4)[c]	1.2 (+15)[c]
0.006[a]	221	10	2.0 (−3)	1.0 (+4)	0.5 (+15)
0.17[b]	218	20	1.5 (−3)	2.6 (+4)	2.6 (+15)
2.7[a]	221	1	1.0 (−2)	8.0 (+4)[c]	1.2 (+15)[c]
2.7[a]	221	10	2.0 (−3)	3.0 (+4)	1.5 (+15)
5.5[b]	218	20	1.5 (−3)	3.0 (+4)	3.0 (+15)

Dilution ratios $\mathcal{D}$ are taken from our model. Plume age t and cumulative aerosol number densities $n_>$ are estimated from the measurements which show a marked variability. In all cases, contrails have formed. The values N(vol) have to be compared with the soot emission index for the ATTAS, which is 1.7×10^{15} soot particles per kilogram fuel. The relationship applied for the ATTAS to evaluate N reads $N = 1.5 \times 10^8 n_>/\mathcal{D}$ in the units as given in the table. Read 1.0 (−2) as 1.0×10^{-2}.

[a] SULFUR 4.

[b] SULFUR 2.

[c] Values must be regarded as lower limits.

during the SULFUR campaigns have clearly shown that N(soot) does not depend on the sulfur content of the kerosene (*Petzold et al.*, manuscript in review, 1998). Although N(vol) exceeds N(soot), no clear trends can be read off these few figures, given the uncertainties in dilution ratios, CN cutoffs, and wake conditions.

The measurements during SULFUR 5 allow more detailed conclusions to be drawn. Especially, a direct comparison is possible between volatile particle formation with and without contrails. (All other data discussed up to now were measured in the presence of contrails.) Details of the measurements are published separately (*F.P. Schröder et al.*, manuscript in preparation, 1998). The instrumentation used was the same as in SULFUR 4, except the particle counter. The CN counters used were different from those employed during earlier missions. The nominal lower cutoff radius of the new instrument was 2.5 nm. It was connected to a dilution system to avoid early saturation at short distances (a few hundred meters past exit) and to allow safe detection of $\sim$ 40 times higher concentrations compared to the previous measurements. (The near-field values shown in Tables 2 and 3 suffered from saturation effects and must be regarded as lower limits.) Also, the sampling line was split into a heated (200°C) and an unheated section to separate volatile and nonvolatiles particles.

We briefly discuss with the help of Figure 8 the flight on April 18, 1997 at 287 hPa, 219 K (upper flight level, with contrail), at a relative humidity around 50 %. Jet fuel was used with either 0.02 g / kg or 2.7 g / kg sulfur content. We focus on the latter case and choose $s = 0.02$ and $n_{ci} = 10^8\,\mathrm{cm}^{-3}$. Engine parameters lead to the same relationship between N and $n_>$ as given in Table 3. Figure 8 depicts the simulated evolution of N(vol) as the total number density of volatile aerosols with $r > 2.5$ nm.

In Figure 8, observed values are indicated as diamonds. (In the measurements without contrail, CN data were higher and reached a constant level around 10^{17} (kg fuel)$^{-1}$ already at $t = 1$ s.) Volatile aerosol levels are generally higher than those shown earlier for $r > 4$ nm (see also Table 3), indicating that the majority of new ultrafine aerosols peaks in the few nanometer size regime. The simulations using $r > 2.5$ nm stay somewhat below the observations. A rapid decrease is seen at $t = 0.2$ s due to the decrease in humidity when the contrail forms, causing H_2O to leave the small particles and shrink below the prescribed size limits. Later, N(vol) decreases further which is mainly caused by scavenging losses of the small particles undergoing collisions with ice particles (see Figure 3, part 1).

The simulated N(vol) values in Figure 8 would change upon variations of s and n_{ci}. Increasing s or n_{ci}, and/or using a lower cutoff radius, would bring the model in better agreement with the observed data. The sensitivity of calculated particle emissions N(vol) (and inferred sulfur conversion efficiencies) on the assumed size limit has been pointed out previously by *Kärcher and Fahey*

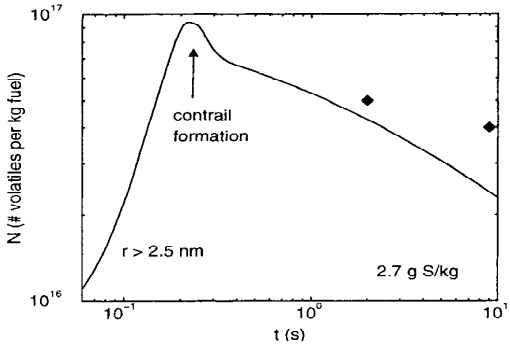

Figure 8. Cumulative number of volatile aerosol particles per kilogram fuel with $r > 2.5$ nm with contrail formation. The plume age where ice particles start to form is indicated by the arrow. The diamonds are representative values measured during SULFUR 5. Observed values in plumes without contrails exceed 10^{17} per kg fuel and show no decreasing trend, indicating longer lifetimes in the atmosphere.

[1997]. Because of the presence of both charged and uncharged particles in the plume, CN counters calibrated with neutral particles could have a smaller detection limit when they count charged particles in a plume. At a given supersaturation level in the CN instrument the nucleation barrier of a charged particle is reduced compared to a neutral particle. This allows the detection of smaller particles up to the point where the increasing Kelvin barrier shuts off further detection of ions. This effect could be important in near-field measurements, when the ionization level of plume aerosols has not yet decayed to background values.

The ability of our model to accurately simulate the cumulative number densities of ultrafine particles is also limited by numerical diffusion, especially when the lower cutoff of the particle counter is at the large size tail of the particle spectrum, because the spectrum falls off very rapidly. This limitation may become serious for (very) low FSCs, such as the N(vol) values for 0.006 g S/kg fuel listed in Table 3, which thus may be lower limits. For (very) high FSCs the mean radius of the spectrum is similar to or larger than the cutoff radius, so the broadening of the size distribution due to numerical diffusion has no significant effect on the evaluation of the cumulative abundances. (In both cases, neutral particles remain too small to be detected.) Reducing or eliminating numerical diffusion would probably require the use of higher ion emissions and/or conversion rates in our model to obtain comparable results in cases with low FSCs.

We finally note that the SULFUR 5 observations performed with 0.02 g S / kg fuel show a reduction of N by about a factor of 10 compared to the data shown in Figure 8; that is, low sulfur values for the ATTAS reach 2×10^{16} volatile particles per kg fuel. These numbers are consistent with results obtained during POLINAT [*Schumann*, 1997] for larger commercial aircraft. These

still high levels of volatile particles for low FSC could also be due to emissions of ions. Chemi-ion production does not require the presence of sulfur molecules [*Yu and Turco*, 1997]. In the absence of sulfur we speculate that the ions might grow by uptake of H_2O together with other condensable species to detectable sizes. Measurements by *Frenzel and Arnold* [1994] showed that for low-sulfur fuel the charged molecular clusters are mainly composed of $NO_3^- \cdot HNO_3$ ions, whereas for FSCs $> 0.2\,g/kg$, the most abundant negative ions were mainly composed of sulfur-derived molecules [*Arnold et al.*, 1998]. Further interpretation of the SULFUR 5 data and details of the particle measurements will be presented elsewhere.

5. Conclusions

5.1. Summary of Results

1. Sulfur emissions are mainly responsible for the formation of new volatile particles in young aircraft plumes. Increasing the sulfur content in the jet fuel directly translates into enhanced growth of these particles in the ultrafine size region. For the ATTAS the abundance of volatile particles in the near field exceeds $10^{16} - 10^{17}$ particles per kg fuel for average to high fuel sulfur levels ($> 0.5\,g\,S/kg\,fuel$), even when the direct emissions of oxidized sulfur (in the form of SO_3) are only a few percent of the total sulfur emissions. The corresponding ratios of volatile to soot particle abundances range between 10 and 100. Particulate H_2SO_4/H_2O formation is consistent with rapid depletion of gaseous H_2SO_4 from the gas phase [*Curtius et al.*, 1998].

2. Chemi-ions formed during the combustion of jet fuel very likely play an important role in the formation of new particles and contrails, and probably also in the activation of exhaust soot, thereby supporting previous results for the Concorde [*Yu and Turco*, 1997]. The present model results for the abundances of ultrafine condensation nuclei come to closer agreement with observations when charged clusters are included in the aerosol dynamics. The presence of chemi-ions in the exhaust can explain the observed, moderate (factor of $2 - 3$) changes of ultrafine CN fractions over a large (factor of 450) span of fuel sulfur contents.

3. Soot particles are expected to acquire at least a partial liquid coating by adsorption of H_2O. The water coating is enhanced and transformed into an aqueous solution by adsorption of oxidized sulfur in the form of SO_3 and H_2SO_4 and by scavenging of freshly nucleated particles. Already at the end of the jet regime, a considerable fraction of the total soot surface area (several tens of percent) can be covered by a liquid coating. The initial sulfur coating will increase with plume age (part 1, Figure 4). This process likely enhances the ice-forming ability of soot in the atmosphere. At the same time, it may decrease the potential of the particles to sustain proposed heterogeneous chemical reactions (on dry surfaces) affecting ozone [*Lary et al.*, 1997; *Bekki*, 1997]. On the other hand, the presence of the coating may allow other reactions to take place.

4. Contrail formation temperatures can be predicted thermodynamically, when ambient relative humidity, temperature, fuel properties, and engine overall propulsion efficiency at a given flight level are known. Contrails form when liquid water saturation is approached or exceeded in the plume and initially consist of more ($10^4\,cm^{-3}$) but smaller ($1\,\mu m$) particles than natural cirrus clouds. Observations and simulations indicate a dependence of volatile aerosol emissions on contrail formation in the sense that fewer (by a factor of $2 - 5$) volatiles are detected when a contrail has formed. This difference is in part tied to coagulation of the small particles with contrail ice crystals that offer a sufficiently large scavenging cross section and to changes in the large tail of the size distribution of the ultrafine aerosols located at the detection limits of CN counters.

5. Ice particles in contrails mainly nucleate on exhaust aerosols. The latter pass a liquid growth stage prior to freezing where they are activated into nearly pure liquid water droplets. At temperatures within about 2 K below the threshold formation temperature and for average fuel sulfur contents or below, coated soot particles very likely dominate the ice formation process. According to the model, lower temperatures and/or higher sulfur levels render homogeneous freezing of volatile plume aerosols more important than heterogeneous freezing of ice in the liquid soot coatings. This causes freezing of about a factor of two more and correspondingly smaller ice particles when the fuel sulfur level is enhanced by two orders of magnitude. Metal particles emitted by jet engines may contribute to the formation of large ($> 1\,\mu m$) ice crystals in contrails due to their large initial size, depending on their ice nucleation ability.

6. Contrails with larger ice crystals would also form without soot and sulfur emissions by activation and freezing of background aerosols entrained into the plume. However, the threshold formation temperatures would be shifted to slightly smaller values, depending on the abundance and freezing properties of the ambient particles. Microphysical parameters of contrails formed within thin cirrus clouds in air near liquid water saturation are different from those formed in clear air. The simulations suggest that natural cirrus clouds can be modified by aircraft exhaust aerosols.

Although soot emission levels, aerosol formation potential, and wake dilution properties may vary, there is no evidence for principal differences between subsonic and supersonic plumes and engines with regard to aerosol microphysical and chemical processes. Except for the mentioned differences in particle evolution with and without contrails, near-field processing is primarily governed by the thermodynamic conditions in the jet plume and only weakly by atmospheric conditions at the flight levels. However, the physicochemical transformation of aviation-produced particles, includ-

ing contrail formation and their impact on atmospheric chemistry and climate parameters, will strongly depend on the cruising altitude.

5.2. Open Issues

The ability of the present model to simulate the dynamics of ultrafine volatile aerosol is limited. Ultimately, the treatment of plume aerosol growth and microphysics including charged particles must be refined to enhance the predictive ability of the model. However, aerosols in this size range also need further characterization by highly resolved size distribution measurements as well as accurate determination of emitted chemi-ion levels. Another open issue concerns the accuracy of CN measurements of nanometer-sized (charged) particles under plume conditions.

Present plume observations are insufficient to answer the question whether there exists a dependence of SO_3 emissions on the fuel sulfur content. To infer such a dependence, one has to assume that the volatile exhaust particles are composed of H_2SO_4/H_2O due to the lack of in situ composition analyses. (To mention one exception, particles have been found to consist of H_2SO_4/H_2O, as demonstrated by *Curtius et al.* [1998] for high-sulfur fuel, in which case sulfur effects are expected to dominate particle formation and growth.) A nonlinear dependence is predicted by simulations of chemical reactions within jet engines [*Brown et al.*, 1996]. If it exists, it would modulate some of the results obtained by varying the fuel sulfur content for fixed SO_3 emissions, but the general findings would likely remain the same.

The low level of directly emitted SO_3 derived from the present comparisons with observations behind the ATTAS are sufficient to explain the observed, high levels of volatile aerosols and the sulfur dependence of the ultrafine condensation nuclei fraction in the exhaust. Low-sulfur conversion rates of the order of 2 % thus seem appropriate at least for the ATTAS engines. Whereas we believe that this statement holds for average and high fuel sulfur contents, the effects of numerical diffusion limit our ability to accurately determine conversion rates in cases with low fuel sulfur levels. It is conceivable that much higher conversion rates must be prescribed in a diffusion-free model to match the low-sulfur observations. For the same reason it also cannot be excluded that particles are composed of condensable material other than H_2SO_4 when the fuel sulfur level becomes reduced.

High emissions of SO_3 are mainly governed by the specific engine design and cannot be ruled out for other jet engines by this work, even for high fuel sulfur levels. The residence time of the exhaust gases in the cooling turbine flow, where most SO_3 is believed to form via reactions of SO_2 with atomic oxygen, is a crucial parameter. The shorter this residence time is, the more formation of SO_3 is suppressed due to kinetic limitations [*Hunter*, 1982].

The present database is also insufficient to further constrain the role of soot in contrail formation. Partly, this arises from a substantial uncertainty in predicting soot emission indices and size distributions. The ATTAS emits 1.7×10^{15} black carbon particles per kg fuel. Emission indices from more modern subsonic jet engines can be similar, or can be smaller by a factor of 10 or more. Other uncertainties are introduced by the freezing properties of fresh exhaust soot, which are only poorly known, and by the application of the "classical" theory to compute heterogeneous freezing rates involving soot.

5.3. Potential Atmospheric Impact of Aviation-Produced Aerosols

We hope that the discussion of open issues as they arise from this work helps defining the directions where future near-field research work should be concentrated. Keeping in mind that uncertainties in the understanding and prediction of aircraft aerosol formation processes remain, the results of the observations in concert with the present analyses suggest a conceivable impact of exhaust aerosols on chemical, radiative, and cloud formation processes in the upper troposphere and lower stratosphere. Emission levels of volatile and soot particles discussed here are high enough to cause potentially relevant perturbations of background surface area densities (see Table 4).

The estimated mean changes in surface area and number density of soot particles (assumed to be spherical) and liquid aerosol particles are obtained using a fuel consumption of $120\,\mathrm{Tg\,yr^{-1}}$ in the northern hemisphere (1992 figure) of which 40 % is consumed in the lowermost stratosphere (air mass 2.3×10^{17} kg according to *Appenzeller et al.* [1996]), a mean residence time of 2 months, an average FSC of 0.4 g / kg, an average soot EI of 0.04 g / kg, and particle mass densities $1.5\,\mathrm{g\,cm^{-3}}$. The assumed emission of volatile (soot) particles is 10^{16} (kg fuel)$^{-1}$ and 2×10^{14} (kg fuel)$^{-1}$, respectively. Although the most recent near-field measurements indicate that 10^{17} (kg fuel)$^{-1}$ volatile particles will become detectable in the aged wake, we use the lower value to account for possible scavenging losses occuring during the residence time of these aerosols in the stratosphere. The nominal value for soot (10^{15} (kg fuel)$^{-1}$) is reduced by a factor of five for the same reason. (Scavenging losses are smaller due to the larger particle size compared to the liquid particles.)

From the prescribed soot emission index we calculate a mass-weighted mean diameter of 65 nm. Further, we assume 5 % oxidation of fuel sulfur and 55 % H_2SO_4 in the droplets, yielding a mass-weighted mean diameter of 25 nm for the H_2SO_4/H_2O droplets. These simple estimates noted in Table 4 clearly show that aircraft emissions may cause substantial changes in CN concentrations and surface area density values. Of course, the background CN abundances themselves exhibit a rather large variability at cruising altitudes.

Table 4. Mean Size and Changes (zonal mean values) of H_2SO_4/H_2O Aerosol (d) and Soot Particle (s) Properties due to Subsonic Aircraft Cruising in the Lowermost Stratosphere.

Perturbed quantity	Value	Unit
Diameter of mean mass (d)	25	nm
Diameter of mean mass (s)	65	nm
Number concentration change (d)	105	cm^{-3}
Number concentration change (s)	2	cm^{-3}
Surface area density change (d)	0.2	$\mu m^2\,cm^{-3}$
Surface area density change (s)	0.03	$\mu m^2\,cm^{-3}$
Mass concentration change (s)	0.4	$ng\,m^{-3}$

The estimated changes have to be compared with typical background values of $200\,cm^{-3}$ and $1\,\mu m^2\,cm^{-3}$ (sulfate aerosols) and $0.1\,cm^{-3}$, $0.01\,\mu m^2\,cm^{-3}$, and $1\,ng\,m^{-3}$ (soot). For further details, see text.

During the final preparation of this paper, we learned that there is a first observational evidence that supports our figures. By analysing a long-term record of ballonborne aerosol data, *Hofmann et al.* [1998] estimated that the contribution of the commercial aircraft fleet amounts to about 10 % of the total particle concentrations measured over Laramie, Wyoming in the altitude band between 9 and 13 km. This value is in good general agreement with the perturbations listed in Table 4.

The enhanced level of volatile aerosol can potentially trigger additional chlorine activation that has been proposed to be efficient even in the midlatitude tropopause region [*Solomon et al.*, 1997]. However, modeling the chemical and microphysical evolution of aviation aerosols at the tropopause will be a difficult task. Exhaust soot particles might influence the formation and evolution of cirrus clouds, although they appear to be relatively inefficient ice-forming nuclei. Here the calculation of aerosol processing in evaporating contrails, where the shrinking ice particles are transformed back to their volatile and nonvolatile cores that may in turn serve as ice nuclei, is a challenging problem. *DeMott et al.* [1990] and *Jensen and Toon* [1997] point out that even poor ice nuclei may affect cloud formation in the upper troposphere, a region which is characterized by very little concentrations (i.e., 1 per liter) of efficient ice nuclei. Our conjecture that a second freezing mode working independently of sulfur probably exists may have important implications for soot and cirrus cloud interaction.

If future research points toward observable atmospheric perturbations related to aviation aerosols, the main strategy should be to prevent soot formation or to minimize its emission and to lower the average sulfur level in jet fuel.

Acknowledgments. The authors benefited from discussions with Olivier Boucher, Michael Danilin, David Fahey, Patrick Minnis, and Brian Toon. This research was supported by the German Federal Ministry of Education and Research (BMBF), by the German Federal Authority of the Environment (UBA), and by the U.S. Subsonic Assessment Program (NASA).

References

Appenzeller, C., J.R. Holton, and K.H. Rosenlof, Seasonal variation of mass transport across the tropopause, *J. Geophys. Res.*, *101*, 15,071-15,078, 1996.

Arnold, F., Th. Stilp, R. Busen, and U. Schumann, Jet engine exhaust chemiion measurements: Implications for gaseous SO_3 and H_2SO_4, *Atmos. Environ.*, in press, 1998.

Bekki, S., On the possible role of aircraft-generated soot in the middle-latitude ozone depletion, *J. Geophys. Res.*, *102*, 10,751–10,758, 1997.

Bockhorn, H. (Ed.), *Soot Formation in Combustion*, Springer–Verlag, New York, 1994.

Brown, R.C., M.R. Anderson, R.C. Miake-Lye, C.E. Kolb, A.A. Sorokin, and Y.I. Buriko, Aircraft exhaust sulfur emissions, *Geophys. Res. Lett.*, *23*, 3603–3606, 1996.

Brown, R.C., R.C. Miake-Lye, M.R. Anderson, and C.E. Kolb, Aircraft sulfur emissions and the formation of visible contrails, *Geophys. Res. Lett.*, *24*, 385–388, 1997.

Busen, R., and U. Schumann, Visible contrail formation from fuels with different sulfur contents, *Geophys. Res. Lett.*, *22*, 1357–1360, 1995.

Busen, R., D. Hagen, M. Kuhn, A. Petzold, F. Schröder, U. Schumann, J. Ström, and P. Whitefield, Experiments on contrail formation from fuels with different sulfur content, in *Proceedings of the International Colloquium on the Impact of Aircraft Upon the Atmosphere*, pp. 149–154, Off. Natl. Etud. et de Rech. Aerosp., Chatillon, France, 1997.

Curtius, J., B. Sierau, F. Arnold, R. Busen, and U. Schumann, First direct sulfuric acid detection in the exhaust plume of a jet aircraft in flight, *Geophys. Res. Lett.*, *25*, 923–926, 1998.

DeMott, P.J., An exploratory study of ice nucleation by soot aerosols, *J. Appl. Meteor.*, *29*, 1072–1079, 1990.

Frenzel, A. and F. Arnold, Sulfuric acid cluster ion formation by jet engines: Implications for sulfuric acid formation and nucleation, *DLR Mitt. 94-06*, pp.106–112, Dtsch. Forschungsanst. für Luft- und Raumfahrt, Köln, Germany.

Freudenthaler, V., F. Homburg, and H. Jäger, Optical parameters of contrails from lidar measurements: Linear depolarization. *Geophys. Res. Lett.*, *23*, 3715–3718, 1996.

Gierens, K., and U. Schumann, Colors of contrails from fuels with different sulfur contents, *J. Geophys. Res.*, *101*, 16,731–16,736, 1996.

Gierens, K., and J. Ström, A numerical study of aircraft wake induced ice cloud formation, *J. Atmos. Sci.*, in press, 1998.

Hofmann, D.J., R. Stone, M. Wood, T. Deshler, and J. Harris, An analysis of 25 years of balloonborne aerosol data in search of a signature of the subsonic commercial aircraft fleet, *Geophys. Res. Lett.*, in press, 1998.

Hunter, S.C., Formation of SO_3 in gas turbines. *J. Engineer. Power, Transactions of the ASME*, *104*, 44–51, 1982.

Jensen, E.J., and O.B. Toon, The potential impact of soot particles from aircraft exhaust on cirrus clouds, *Geophys. Res. Lett.*, *24*, 249–252, 1997.

Jensen, E.J., O.B. Toon, S. Kinne, G.W. Sachse, B.E. Anderson, K.R. Chan, C. Twohy, B. Gandrud, A. Heymsfield, and R.C. Miake-Lye, Environment conditions required for contrail formation and persistence, *J. Geophys. Res.*, *103*, 3929–3936, 1998.

Kärcher, B., Physicochemistry of aircraft-generated liquid aerosols, soot, and ice particles, 1, Model description, *J. Geophys. Res.*, this issue.

Kärcher, B., and D.W. Fahey, The role of sulfur emissions in volatile particle formation in jet aircraft exhaust plumes, *Geophys. Res. Lett.*, *24*, 389–392, 1997.

Kärcher, B., Th. Peter, and R. Ottmann, Contrail formation: Homogeneous nucleation of H_2SO_4 / H_2O droplets, *Geophys. Res. Lett.*, *22*, 1501–1504, 1995.

Kärcher, B., Th. Peter, U.M. Biermann, and U. Schumann, The initial composition of jet condensation trails, *J. Atmos. Sci.*, *53*. 3066–3083, 1996.

Kotzick, R., U. Panne, and R. Niessner, Changes in condensation properties of ultrafine carbon particles subjected to oxidation by ozone, *J. Aerosol Sci.*, *28*, 725–735, 1997.

Langner, J., and H. Rodhe, A global three-dimensional model of the tropospheric sulfur cycle, *J. Atmos. Chem.*, *13*, 225–263, 1991.

Lary, D.J., R. Tuomi, A.M. Lee, M. Newchurch, M. Pirre, and J.B. Renard, Carbon aerosols and atmospheric photochemistry, *J. Geophys. Res.*, *102*, 3671–3682, 1997.

Minnis, P., D.F. Young, L. Ngyuen, D.P. Garber, W.L. Smith Jr., and R. Palikonda, Transformation of contrails into cirrus during SUCCESS, *Geophys. Res. Lett.*, in press, 1998.

Petzold, A., and F.P. Schröder, Jet engine exhaust aerosol characterization, *Aerosol Sci. Technol.*, *28*, 63–77, 1998.

Petzold, A., *et al.*, Near field measurements on contrail properties from fuels with different sulfur content, *J. Geophys. Res.*, *102*, 29,867–29,880, 1997.

Petzold, A., J. Ström, S. Ohlsson, and F.P. Schröder, Elemental composition and morphology of ice crystal residual particles in cirrus clouds and contrails, *Atmos. Res.*, in press, 1998.

Schumann, U., Particle formation in jet aircraft exhausts and contrails for different sulfur containing fuels, in *Nucleation and Atmospheric Aerosols 1996*, edited by M. Kulmala and P. Wagner, pp. 296–299, Elsevier Sci., New York, 1996a.

Schumann, U., On conditions for contrail formation from aircraft exhaust, *Meteorol. Z.*, *5*, 4–23, 1996b.

Schumann, U., J. Ström, R. Busen, R. Baumann, K. Gierens, M. Krautstrunk, F. Schröder, and J. Stingl, In situ observations of particles in jet aircraft exhausts and contrails for different sulfur-containing fuels, *J. Geophys. Res.*, *101*, 6853–6869, 1996.

Schumann, U. (Ed.), Pollution from aircraft emissions in the North Atlantic flight corridor (POLINAT), Air Pollution Research Rep. 58, *EUR 16978 EN*, European Commission, 1997.

Schumann, U., H. Schlager, F. Arnold, R. Baumann, P. Haschberger, and O. Klemm, Dilution of aircraft exhaust plumes at cruise altitudes, *Atmos. Environ.*, in press, 1998.

Solomon, S., S. Borrmann, R.R. Garcia, R. Portmann, L. Thomason, L.R. Poole, D. Winker and M.P. McCormick, Heterogeneous chlorine chemistry in the tropopause region, *J. Geophys. Res.*, *102*, 21,411–21,429, 1997.

Ström, J., and S. Ohlsson, Real-time measurements of absorbing material in contrail ice using a counterflow virtual impactor, *J. Geophys. Res.*, *103*, 8737–8741, 1998.

Thompson, A.M., R.R. Friedl, and H.L. Wesoky, Atmospheric effects of aviation: First report of the subsonic assessment project, *NASA Ref. Publ. RP-1385*, 1996.

Yu, F., and R.P. Turco, The role of ions in the formation and evolution of particles in aircraft plumes, *Geophys. Res. Lett*, *24*, 1927–1930, 1997.

R. Busen, B. Kärcher, A. Petzold, F.P. Schröder, U. Schumann, DLR, Institut für Physik der Atmosphäre, D–82234 Wessling, Germany. E.J. Jensen, NASA Ames Research Center, Mail Stop 245-5, Moffett Field, CA 94035, USA. e-mail: bernd.kaercher@dlr.de.

(Received October 16, 1997; revised March 18, 1998; accepted March 20, 1998.)